

Phytoplankton deposition to permeable sediments under oscillatory flow: Effects of ripple geometry and resuspension

Conrad A. Pilditch^{a,*}, Douglas C. Miller^b

^a*Department of Biological Sciences, University of Waikato, Private Bag 3105, Hamilton, New Zealand*

^b*College of Marine Studies, University of Delaware, 700 Pilottown Rd, Lewes, DE 19958-1298, USA*

Received 20 October 2005; received in revised form 1 May 2006; accepted 1 June 2006

Available online 31 July 2006

Abstract

Pressure-gradient driven, advective flows through permeable sediments are recognized as an important mechanism by which dissolved and particulate materials are exchanged between the near-bottom water and the seabed. Here, we focus on the deposition of particulate organic matter in wave-formed, rippled beds representative of permeable coastal ocean sediments. In addition, we examine the release of previously deposited material when sediment transport is initiated. Laboratory experiments were conducted in an oscillatory water tunnel using cultured diatoms (4–6 μm dia.) as a tracer for particulate organic matter. Using different ripple geometries on a coarse sand bed (median dia. = 575 μm) and following deposition under controlled flow conditions, we cored extensively to determine the distribution and flux of diatoms to the bed. Results showed greater diatom deposition ($3.5 \times$) and penetration depths (4–5 cm) in ripple troughs in comparison to ripple crests (<2 cm), qualitatively in agreement with past model predictions and experimental results. Both this pattern and the total diatom flux were consistent over a 3-fold variation in ripple wavelength (17–50 cm) and a 4-fold variation in ripple height (1.4–7.7 cm). The total diatom flux was only marginally enhanced by the presence of ripples ($\sim 1.6 \times$) compared to a flat bed. Our data suggest that the total diatom flux may be less controlled by rippled bed topography than solute exchanges, including but not limited to advective porewater flows. Repeatability between replicate depositional runs allowed us to conduct resuspension experiments in which rippled beds previously impregnated with diatoms were eroded and allowed to establish a new ripple configuration. Approximately half (45–60%) of the embedded diatoms were released during reconfiguration of the ripples, a process that lasted 20 min. Remaining diatoms were buried comparatively deeper in isolated pockets, the location a function of ripple position both before and after sediment resuspension. Our results clearly indicate that small particle deposition to a rippled bed is a simple pattern predicted by models and prior experiments but that the total flux is not strongly determined by ripple geometry. However, the net depositional pattern in the real ocean will be determined by the combined effects of local sediment erosion and deposition, and thus these two processes act in tandem to lead to substantial, ripple-scale heterogeneity of organic matter input to shelf sediments in both the horizontal and vertical dimensions.

© 2006 Elsevier Ltd. All rights reserved.

Keywords: Particulate organic matter; Deposition; Sediment transport; Surface gravity; Waves; Sand ripples; Bedforms

*Corresponding author. Tel.: +64 7 838 4466; fax: +64 7 838 4321.

E-mail addresses: c.pilditch@waikato.ac.nz (C.A. Pilditch), dmiller@udel.edu (D.C. Miller).

1. Introduction

Processes affecting the deposition and resuspension of particulate organic matter (POM) play a crucial role in shelf ecosystem dynamics. For example, on continental shelves between 25% and 92% of the primary production settles as POM to the seafloor where it is eventually mineralized or buried (Riley, 1956; Jørgensen et al., 1990). This flux is quantitatively significant since the subsequent return of decomposition products to the water column may account for 20–82% of the nitrogen required by phytoplankton (Canfield et al., 1993; Nedwell et al., 1993). Thus, shelf sediments act as a site of substantial nutrient cycling, and a tight coupling exists between the benthic and pelagic environments (Berner, 1980). On high-energy shelves, tides, waves and wind-generated bottom currents cause frequent sediment erosion, deposition and lateral transport (Harris and Coleman, 1998). Consequently, POM can go through many cycles of deposition and resuspension before complete mineralization or burial. Spatial and temporal variations in the flux of POM to sediments will not only affect the mineralization rates but may also be a key determinant of benthic macrofaunal and meiofaunal communities (VanBlaricom, 1982; Snelgrove and Butman, 1994) which rely on energy derived from pelagic production (Hargrave, 1973).

The transfer of POM from the water column to the sediment surface may occur via several mechanisms, including gravitational settling (Fries and Trowbridge, 2003), filtration activities of benthic animals (Graf and Rosenberg, 1997; Miller et al., 2002) and aggregation at the sediment–water interface (Stolzenbach et al., 1992). The interaction of the near-bed flows with microscale topography such as ripples and biogenic structure (e.g. pits, shells and tubes) may also enhance deposition nearby (Eckman, 1990; Yager et al., 1993; Pilditch et al., 1998) by creating regions of reduced shear stress. In addition, for the permeable sediments that characterize coastal areas (Riggs et al., 1996) and cover approximately 70% of the shelf (Emery, 1968), advective porewater exchange driven by horizontal pressure gradients has been identified as a key process influencing POM deposition and solute fluxes (Huettel et al., 1996).

This phenomenon, wherein exchange is enhanced by the pressure gradients generated by boundary layer flows interacting with sediment topography, has received considerable attention (e.g. Webb and

Theodor, 1968; Thibodeaux and Boyle, 1987; Huettel et al., 1996; Precht and Huettel, 2003). Immediately upstream of a structure, the pressure increases as the flow detaches from the bed and as the flow accelerates over the structure a region of low pressure forms (i.e. the Bernoulli Effect). These horizontal pressure gradients produce fluid transport across the sediment–water interface, enhancing the penetration of solutes in the region of high pressure. The rate of advective porewater exchange is strongly determined by sediment permeability and the magnitude of the pressure gradient, which is a function of the height of the roughness element and near-bed flow speed (Huettel et al., 1996). In addition to the fluid and dissolved constituents, this transport process provides a rapid pathway for the transport of POM and phytoplankton into permeable sediments (Pilditch et al., 1998; Huettel and Rusch, 2000; Ehrenhauss et al., 2004a). Coupled with the simultaneous transport of oxygen into the bed (Precht et al., 2004), permeable bed flows enhance the rapid mineralization of this material (Forster et al., 1996).

On continental shelves, surface gravity waves represent a significant component of water motion at the seabed (Dean and Dalrymple, 1992) and consequently sediment transport (Sleath, 1984). Several recent studies have quantified the effects of surface gravity waves on advective porewater exchange confirming that it is an effective transport mechanism (Precht and Huettel, 2003, 2004; Precht et al., 2004; Reimers et al., 2004). Relative to molecular diffusion, the interaction between oscillatory flow and ripples resulted in a 50-fold increase in the fluid exchange under conditions representative of shelf environments (Precht and Huettel, 2003). That study also confirmed previously modelled porewater trajectory paths (Shum and Sundby, 1996) with fluid exiting the permeable bed on ripple crests (low-pressure region) and entering in the troughs (region of high pressure). However, it is difficult to infer rates of POM and phytoplankton deposition from these studies of porewater transport because of natural particle properties such as variable buoyancy, complex morphology and stickiness (Smayda, 1970; Walsby and Reynolds, 1980). Furthermore, while POM deposition may be expected to occur in the troughs in accordance with porewater trajectories, sediment resuspension has the potential to rapidly alter the POM content and spatial distribution within the sediment (Jenness and Duineveld, 1985; Grant et al., 1986, 1997).

Small-scale variations in the distribution of POM can impact trophic interactions by concentrating mobile meiofauna (Hogue and Miller, 1981; Ölafsson, 1991) and acting as sites for mineralization within the sediments (Jørgensen, 1977; Fenchel, 1996; Middelboe et al., 2003). In energetic shelf environments, advective porewater exchange, processes unique to particulate transport (e.g. Fries and Trowbridge, 2003), as well as bulk sediment transport are all likely to play a critical role governing the flux of POM to the sediments and its spatial distribution (Precht and Huettel, 2003).

The aim of this study was to quantify the affects of oscillatory flows on the flux of phytoplankton to a permeable bed with different ripple geometries. In a laboratory water tunnel, the distribution of bed diatoms (our tracer for phytoplankton POM) was determined after a 16-h depositional period to a flat bed, a small rippled bed and a large rippled bed. We hypothesized that total bed diatom concentration (in terms of amount per area of bed) would be positively correlated with ripple size and enhanced in ripple troughs compared to crests consistent with wave-induced advective porewater velocities (Shum and Sundby, 1996). We also quantified the effects of sediment transport on bed diatom distribution and concentration. Our results indicate that although deposition is a simple pattern predicted by models and past experimental work, the flux is less strongly affected by bedforms, and that the overall resulting pattern in the real ocean will be determined by local sediment erosion, deposition and accompanying variation in seafloor microtopography.

2. Methods

2.1. Water tunnel

All experiments were conducted in the Lofquist oscillatory water tunnel described previously by Turner and Miller (1991). Briefly, the water tunnel is U-shaped, with a 350 cm long \times 21 cm wide \times 30 cm deep acrylic horizontal section joining pairs of cylinders that form the vertical arms. The working area consists of a 255 cm long \times 30 cm deep sediment tray that extends the full width of the tunnel and is located centrally in the horizontal section. At the drive end of the tunnel, a variable speed motor causes the pistons to move up and down in the vertical cylinders. When the pistons descend, water is forced through the working section into a turning section and up into the reservoir cylinders at the

opposite end. When the pistons ascend in the drive cylinders, seals on the pistons cause water to be drawn up into the drive cylinders and flow is reversed. At the entrance to either end of the horizontal section, flow is rectified by honeycomb diffusers (5 cm length, 0.25 cm dia.). By adjusting the piston stroke length and the period of oscillation, a wide range of naturally occurring waves (representing wave orbital excursion $<$ 1.5 m, period 3–30 s) can be simulated in the laboratory.

Flow conditions (maximum freestream velocity u_{bmax} and near-bottom excursion semi-amplitude A_b) in the water tunnel are derived from empirical calibration equations based on the piston stroke length and period of oscillation (see Miller et al. (1992) for calculation details). No similar calibration exists to describe the pressure fluctuations in the tunnel so this was measured directly using manometer tubes. Identical lengths of flexible tubing (6.4 mm internal dia.) were attached to ports (4.8 mm dia.) located 13 cm beyond the sediment tray (distance between ports = 281 cm). The tubes were mounted vertically beside the centre of the working section where the fluctuations in the water levels were recorded visually to \pm 1 mm for the different flow treatments (see below). We joined the free ends of the tubes to more readily observe any pressure differential along the working section between the manometer ports.

2.2. Sediment and bed properties

The sand was obtained from dunes at Cape Henlopen, Delaware, USA (38°47.1' N 75°06.1' W) and was chosen because of its similarity to that found on many temperate continental shelves (e.g. Black and Oldman, 1999; Traykovski et al., 1999; Trembanis et al., 2004). Prior to use in the water tunnel, the sand was washed through a 1-mm sieve to eliminate large grains, then rinsed several times with filtered seawater to remove the minimal silt/clay fraction. The same sand was used in all experiments and before each reuse was thoroughly washed, first in fresh water, then in filtered seawater to remove diatoms. At the end of each experiment, sediment grain size was determined using standard sieving techniques, and over the course of our experiments, it did not vary substantially from a median grain diameter of 575 μ m and a quartile deviation of 150 μ m. This sand has an estimated critical erosion velocity (u_{*crit}) of 1.8 cm s⁻¹ based on Shield's curve and a lightly compacted

permeability of 0.2 cm s^{-1} as determined using a constant head permeameter (Klute and Dirksen, 1986). Sediment porosity was measured to 5 cm depth at 0.5 cm intervals with a 1-mm resolution either on the crests or in the troughs for the rippled bed treatments and at several randomly chosen locations for the flat bed. A resistivity probe (Andrews and Bennett, 1981) was used, and since overlying and porewater salinities were identical, no additional adjustment was needed to relate resistance to porosity. We found typical values for sands (e.g. Jackson et al., 1978) and minimal spatial variation (ripple-crest and with depth) as we had expected from using a uniform grain size in our experiments. Specifically, porosity $((R_{(0)}/R_{(z)})^{0.5}$ where $R_{(0)}$ is the resistivity at the surface, $R_{(z)}$ is the resistivity in the sediment at depth z) did not vary appreciably with depth below the top cm and ranged from 0.49 to 0.55 (mean, 0.52 ± 0.02 s.d., $n = 25$) with apparently slightly higher values associated with ripple troughs.

A digital camera (Olympus D-340R) was used to record changes in bed geometry and the location of the subsequent sediment sampling. The camera was positioned level with the centre of the tunnel 1.77 m away from the side wall so that the working section encompassed the entire field of view. Photographs were taken every few minutes during ripple formation and at the end of the experiment when the syringe cores were in place. These images allowed us to accurately locate cores in the horizontal dimension along the water tunnel axis. The images were corrected for radial and tangential lens distortions (Heikkila and Silven, 1996) then rectified using the colinearity equations and the known location of 15 control points scattered throughout the image (Slama et al., 1980). From the rectified images, ripple height (trough–crest) and wavelength (crest–crest and trough–trough) were measured using digitizing software (Image Pro Plus). These measurements provided an accurate representation (horizontal position to ± 0.5 cm, vertical position to ± 0.2 cm) of the bed geometry due to the highly two-dimensional nature of the ripples (described below).

2.3. Diatom tracer of POM

The planktonic diatom *Chaetoceros gracilis*, a common coastal species (Guillard and Kilham, 1977), was used as a tracer of organic matter penetration into the permeable sand bed. Concen-

trated ($\sim 1.8 \times 10^6 \text{ cell mL}^{-1}$) cultures were obtained from Instant Algae[®] Microalgae Products at regular intervals and kept refrigerated in the dark for a maximum of 3 weeks prior to use. Spines normally present on this species had been removed during the culture process resulting in cells with a 4–6 μm diameter. These cultures are normally supplied as an aquaculture feed product, and cells are >99% intact (verified with microscope examination). Algae were added to the tunnel following the preparation of the sand bed and then the stroke and motor speed set to a non-eroding flow condition (see next section). Although the initial concentrations of suspended diatoms (100–150 $\mu\text{g chl } a \text{ L}^{-1}$; Table 1) were 20–100 times higher than that typically observed in temperate continental shelf waters (e.g. Horne et al., 1989; Zeldis et al., 2005), these values were necessary to ensure that measurable levels of diatoms were retained in the bed at the end of an experiment. All experiments were conducted overnight, in the dark (covered by a black plastic sheet) at temperatures of 28–30 °C, and with 30‰ seawater collected from the mouth of the Indian River Inlet, DE, USA. The decline in water column chlorophyll *a* (chl *a*) concentration was determined periodically by filtering duplicate water samples through Whatman GF/F filters then analysing the filters fluorometrically after overnight acetone extraction (Parsons et al., 1984). Microscopic examination of cells suspended in the water and from the sediment confirmed that the mixing in the tunnel did not cause high levels of cell breakage. Preliminary experiments conducted in well-mixed buckets demonstrated that the in vivo and extracted fluorescence to cell number ratio remained constant for at least 16 h. This indicates that cells retained within the bed were not a product of in situ cell division and that chl *a* measurements could be used as an estimate of bed diatom concentration.

2.4. Deposition experiments

To examine the effect of ripple geometry on diatom deposition, we measured the uptake of chl *a* by a well-sorted coarse sand bed that was either flat, had small flow-generated ripples (height (η) = 1.2 cm and wavelength (λ) = 17.2 cm) or had large ripples (η = 3.9 cm, λ = 42.5 cm), and these served as our first three experimental treatments (Table 1). We used one flow setting to produce the ripples and another, non-eroding flow to measure the uptake of diatoms by the bed during a 15–16 h depositional

Table 1

Summary of the sand bed ripple geometry in the sampled portion of the water tunnel and the initial and final diatom (*Chaetoreros gracilis*) concentration ($\mu\text{g chl } a \text{ L}^{-1}$) in the water at the start and end of deposition and resuspension experiments

Treatment/run	# of ripples	Bed geometry				Tunnel chl <i>a</i> conc		Experiment duration (h)
		λ		η		Initial ($\mu\text{g chl } a \text{ L}^{-1}$)	Final ($\mu\text{g chl } a \text{ L}^{-1}$)	
		Initial (cm)	Final (cm)	Initial (cm)	Final (cm)			
<i>Deposition experiments</i>								
Flat bed 1	—	—	—	—	—	125	59	16.0
Flat bed 2	—	—	—	—	—	118	51	15.2
Small ripple 1	9	17.5 \pm 2.8	17.5 \pm 3.4	1.7 \pm 0.6	1.2 \pm 0.4	102	48	15.3
Small ripple 2	9	17.1 \pm 2.8	16.9 \pm 3.6	1.4 \pm 0.4	1.2 \pm 0.4	91	54	16.5
Large ripple 1	4	35.6 \pm 9.4	35.7 \pm 8.1	5.6 \pm 1.8	3.1 \pm 1.2	111	49	16.1
Large ripple 2	3	50.1 \pm 4.1	50.1 \pm 5.5	7.7 \pm 1.6	4.7 \pm 1.2	99	54	15.1
<i>Resuspension experiments</i>								
Resuspension 1								
Small ripples – deposition	10	15.1 \pm 3.6	15.2 \pm 3.9	1.4 \pm 0.5	0.9 \pm 0.3	108	58	15.5
Large ripples – resuspension	4	—	34.1 \pm 6.1	—	4.7 \pm 1.5	8	21	0.5
Resuspension 2								
Small ripples – deposition	10	14.5 \pm 3.4	15.6 \pm 4.2	1.2 \pm 0.3	0.9 \pm 0.3	125	54	16.1
Large ripples – resuspension	4	—	39.3 \pm 5.3	—	5.2 \pm 0.8	13	28	0.3

λ = ripple wavelength, η = ripple height (trough to crest) and values represent means \pm 1 s.d.

period. First, a piston stroke length of 25 cm and period of 8.8 s (resulting in u_{bmax} of 44 cm s⁻¹ and semi-amplitude A_b of 61 cm) generated small ripples in a flat bed after 6–7 min and larger ripples after 16–20 min. Due to the narrow width of the tunnel compared to its length, the ripples were highly two-dimensional (Lofquist, 1977) and reproducible between replicate runs of the same treatment (see Table 1). When viewed from the side through the clear acrylic walls, ripples generated in the water tunnel extended directly from the walls across the working section with little (< few millimetres) deviation in height or crest-line position across the channel. We interpret the observed uniformity of the bedforms to indicate minimal cross-channel flow artifacts, and this inference is consistent with the thin nature of oscillatory boundary layers present along the smooth, acrylic sidewalls. We observed this highly two-dimensional nature of the ripples regardless of the imposed flow, sediment grain size or resulting bedform dimensions (e.g. Miller et al., 1992).

Next, for the depositional phase, the stroke length was decreased to 12 cm and the period increased to 13.5 s which resulted in $u_{bmax} = 13.7 \text{ cm s}^{-1}$, $A_b = 29.4 \text{ cm}$. To circumvent any unrecognized potential flow artifacts associated with the water tunnel design (e.g. limited boundary layer develop-

ment, secondary flow patterns; see Nowell and Jumars, 1984), we included controls, replication (i.e. each bed treatment was run twice) and extensive sampling of the bed (three positions across the channels on crests and troughs, and 16–33 midline positions, e.g. as indicated in Figs. 1 and 2) for deposited diatoms throughout (along and across) the working section. The flat bed treatment acted as a flow control allowing the quantification of depositional patterns in the absence of advective processes driven by oscillating flows interacting with sediment topography. Because these resulting depositional patterns integrated any flow artifacts due to the small size of the wave tank, we could adequately distinguish patterns caused by the rippled bed treatments and any resulting from the wave tank design. Since bed profiles were uniform across the working section in every case, we assume that if unrecognized flow artifacts were present along or across stream that they did not vary with treatment.

Prior to each run (eight in all, four treatments with two replicates of each), a flat sand bed was prepared in the sediment tray insert (25 cm deep) that ran the entire length and width of the working section. The tray was filled to a depth of 5 cm with 3–5 mm diameter pea gravel, covered with a plastic liner then filled two-thirds full with seawater filtered

Table 2

Summary of the final bed chl *a* concentration derived from syringe cores equally spaced between ripple crests and troughs along the centre of the water tunnel working section

Treatment/run	Treatment mean ($\mu\text{g chl } a \text{ cm}^{-2}$)	Location				
		Trough ($\mu\text{g chl } a \text{ cm}^{-2}$)	Near-trough ($\mu\text{g chl } a \text{ cm}^{-2}$)	Mid crest- trough ($\mu\text{g chl } a \text{ cm}^{-2}$)	Near-crest ($\mu\text{g chl } a \text{ cm}^{-2}$)	Crest ($\mu\text{g chl } a \text{ cm}^{-2}$)
<i>Deposition experiments</i>						
ANOVA <i>p</i>	< 0.001	> 0.8			< 0.001	
Flat bed 1	0.81 ± 0.14 (16) ^a	—	—	—	—	—
Flat bed 2	0.79 ± 0.17 (16) ^a	—	—	—	—	—
Small ripple 1	1.29 ± 0.47 (33) ^b	1.79 ± 0.16 (8)	—	1.40 ± 0.10 (16)	—	0.64 ± 0.07 (9) ^a
Small ripple 2	1.29 ± 0.54 (34) ^b	1.76 ± 0.38 (10)	—	1.37 ± 0.35 (15)	—	0.61 ± 0.11 (9) ^a
Large ripple 1	1.32 ± 0.57 (25) ^b	1.94 ± 0.36 (5)	1.73 ± 0.40 (8)	—	1.04 ± 0.28 (8)	0.43 ± 0.09 (4) ^b
Large ripple 2	1.25 ± 0.51 (25) ^b	1.81 ± 0.23 (4)	1.52 ± 0.15 (6)	1.24 ± 0.17 (6)	0.73 ± 0.09 (6)	0.40 ± 0.05 (3) ^b
<i>Resuspension experiments</i>						
Resuspension 1	0.55 ± 0.30 (28)	0.31 ± 0.06 (5)	0.47 ± 0.15 (9)	—	0.61 ± 0.35 (9)	0.79 ± 0.37 (5)
Resuspension 2	0.71 ± 0.45 (28)	0.38 ± 0.03 (4)	0.45 ± 0.10 (8)	0.53 (2)	0.78 ± 0.33 (8)	1.34 ± 0.53 (5)

The results of a one-way ANOVA (significant values in bold) and post-hoc Tukey tests examining differences in chl *a* concentration among deposition treatment/runs are also given. Treatment/runs sharing the same letter were not significantly different in the post-hoc tests ($p > 0.05$). Values are vertically integrated means ± 1 s.d. with the number of syringe cores in parentheses.

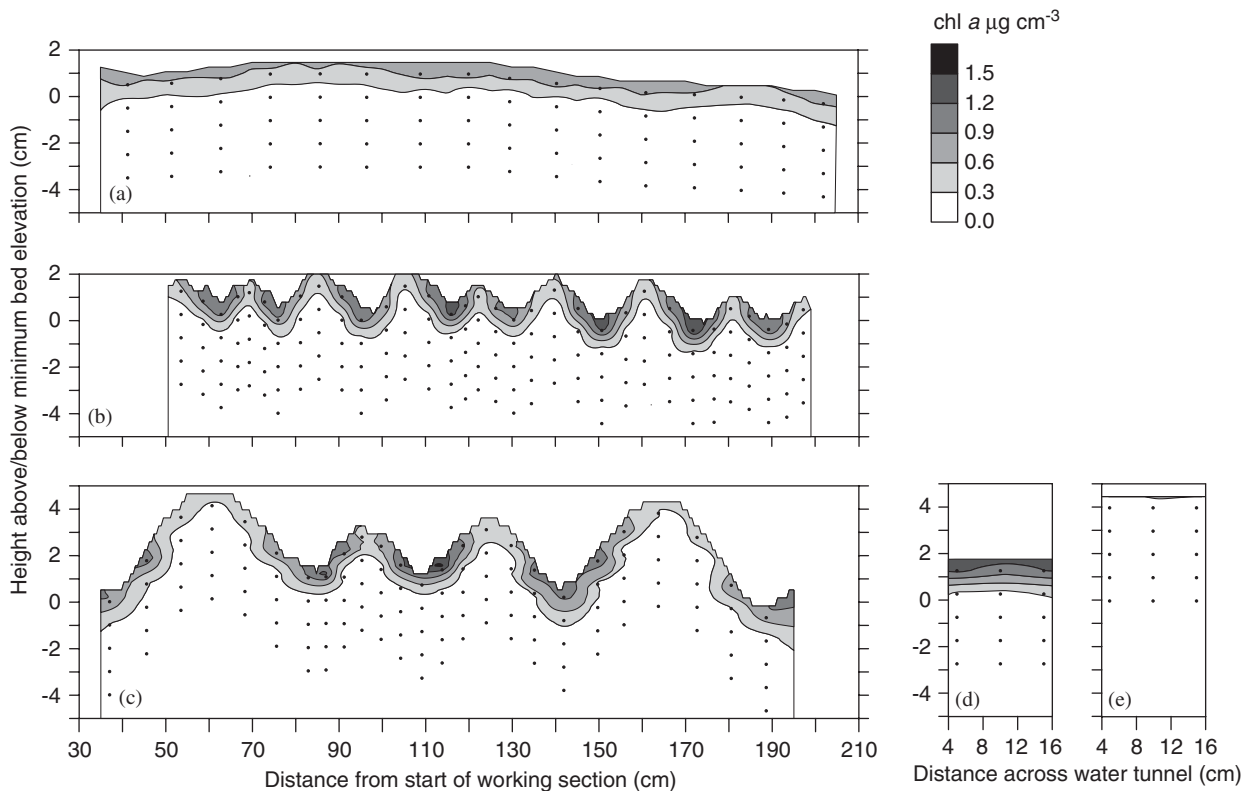


Fig. 1. Contour plots of the vertical distribution of sediment chl *a* at the end of deposition experiments to beds with contrasting ripple geometry; (a) flat bed, (b) small ripples and (c) large ripples. Cross-stream variation in deposited chl *a* in a large ripple trough (d) and on a large ripple crest (e). The plots were compiled from vertically sectioned sediment cores at the locations indicated by the black dots. To aid direct comparison, identical vertical scales are used in each plot.

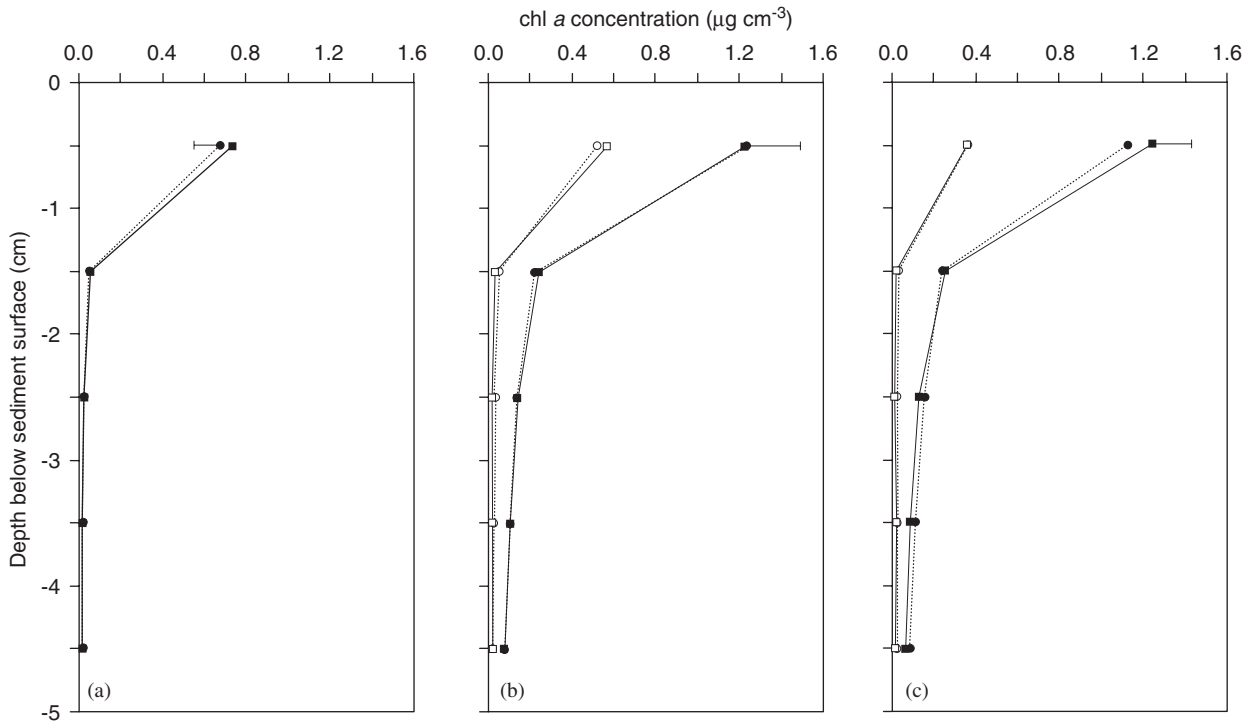


Fig. 2. Penetration depth of chl *a* at the end of deposition experiments to a flat bed (a) and in the trough (solid symbols) and on the crests (open symbols) of a small (b) and large (c) rippled bed. In each plot, the circle and square symbols refer to replicate experiments. Data represent the means of 4–16 sediment cores (see Table 2) and for clarity only the maximum s.d. has been shown, whereas the minimum s.d. is within the size of the symbol.

to 2 μm . Sand was then added, compacted by hand and smoothed flush with the bottom of the working section. The tunnel was then sealed, filled with filtered seawater and for six of the eight treatments small or large ripples generated as described above. The depositional run proper was initiated by adding algae, then setting the stroke and the motor speed to the non-eroding flow condition.

At the termination of each overnight run, the water tunnel motor was switched off and the water level slowly reduced to 5 cm above the bed by a siphon maintained just below the water surface to avoid any disturbance to the bed. To obtain samples of bed chl *a* concentration, 35–45 truncated 10-mL syringe cores (cross sectional area = 1.62 cm²) were inserted into the sand to a depth of 6 cm. Most of these cores were placed in a line along the centre of the working section. We restricted our sampling in the working section to the middle 2 m of the area between the honeycomb entrance diffusers to minimize any impacts associated with the entrance and exit conditions. The exact position of the cores along this midline varied among runs due to

variations in the location of ripple crests and troughs. At selected locations cross-stream, variations in depositional patterns were assessed by placing an additional core midway between the midline cores and the tunnel walls. Sediment cores were sectioned vertically at 1 cm intervals, frozen and analysed fluorometrically for chl *a* within 1 week. In preliminary still-water settling trials conducted under identical conditions but conducted in plastic buckets, diatoms were allowed to settle overnight to a sand bed. Chl *a* was only detected in the surface layer (0.0–0.5 cm) indicating that cells were negatively buoyant and that our coring methods did not smear the vertical distribution. Furthermore, regular sampling of the water column indicated that passive deposition of cells that occurs in the short interval (~20 min) between the water drained to the time all the cores were in place would account for <5% of the chl *a* in the surface (0–1 cm) layer. Thus, this passive deposition did not contribute substantially to the measured diatom fluxes and did not appreciably affect distribution patterns.

2.5. Resuspension experiments

Because of the repeatability both in ripple morphology and diatom deposition (see Section 3), we were able to create a known, diatom-impregnated bed that we subsequently eroded and cored to determine any effects of the sediment transport event. Specifically, we allowed deposition to a small rippled bed (overnight, as above), then increased the flow (as above) to generate bedforms comparable in ripple height and wavelength to those on the large rippled bed experiments. As with previous treatments, this one was also replicated twice. Between the depositional and erosion phases, water in the tunnel was siphoned off to within 5 cm of the bed (removing most of the suspended and undeposited POM), then the tunnel re-filled with filtered seawater. This reduced the suspended chl *a* concentration by 5–10 × allowing us the opportunity to detect any change in concentration resulting from the resuspension of bed diatoms. The water in the tunnel was allowed to mix for 10 min at the non-eroding flow before altering the piston stroke and period to initiate the erosion phase. We then allowed the bed to evolve to the large ripple configuration (15–20 min, taking sequential bed photographs as described above) before stopping the experiment and coring the bed. In order to detect diatoms that may have been buried deeply by ripple migration/formation, the core depth was increased to 10 cm (by doubling the core length) and sectioned as before at 1 cm intervals. Diatom concentration in the water column was measured during the resuspension experiment by recording *in vivo* fluorescence 30 cm above the bed. A peristaltic pump (flow rate = 3 L min⁻¹) recirculated water from the water tunnel through a Turner design fluorometer and the fluorescence was logged every 10 s. The ratio of fluorescence to chl *a* concentration was calibrated from water samples taken during the resuspension period.

2.6. Statistical analysis

Preliminary analysis of flat bed syringe chl *a* (in µg chl *a* cm⁻³) values indicated no along-tunnel gradients or depositional patterns associated with entrance conditions, and we therefore treated syringe cores as independent replicates. For rippled beds, we classified cores according to the bed profile where collected, i.e. ripple crest, trough or some point in between (Table 2). A one-way analysis of

variance (ANOVA) was used to detect significant differences ($p < 0.05$) in the vertically integrated chl *a* concentration values (in µg chl *a* cm⁻²) amongst the six deposition runs (two replicates each of the flat, small and large rippled beds) and homogenous subsets identified using Tukey's post-hoc test. In our analysis, we treated each run as a separate treatment (i.e. there were two replicates of each bed type) and used the post-hoc tests to determine where significant differences occurred. The same approach was used to determine if bed diatom deposition to crests or troughs differs amongst rippled bed runs. Data were checked for normality and homogeneity of variance by visual inspection of residuals and no transformations were necessary. All tests were conducted using SPSS version 11.5 (SPSS, Inc., Chicago, IL).

3. Results

3.1. Pressure fluctuations in the water tunnel

Absolute pressure in the working section is essentially hydrostatic, determined mainly by the water level in the open cylinder end (Lofquist, 1977, and personal observations, 2003). As expected, the water level in the manometer tubes from both ends fell and rose with the free surface in the open cylinders and in opposite phase to that of the drive pistons. This temporal variation in hydrostatic pressure was subsequently confirmed with a pressure sensor (Paroscientific, Redmond, WA) placed in the middle of the working section. At the flow settings used for the overnight depositional periods, there was also a spatial gradient in pressure along the working section that resulted in drive cylinder end manometer tube level varying 1.8–2.0 cm over the 281 cm working section. Although larger differential pressures (up to 12 cm) were observed for the flow conditions for ripple generation, these are not relevant since they were temporarily present during ripple formation and not during deposition periods when diatoms were introduced into the water column for deposition into the sediment.

3.2. Effect of ripples on diatom deposition and distribution

For each treatment, the number of ripples, and the mean ripple height (η) and wavelength (λ) were relatively consistent between replicate experiments (Table 1). For the small ripple treatment, mean λ

was ~ 17 cm and mean η was 1.2–1.7 cm, whereas for the large ripple treatment, average λ ranged from 36 to 50 cm and η from 3.1 to 7.7 cm along the working section. Thus, the small ripple density was approximately $3 \times$ greater than for the large ripple treatment, but η was only one-third the height of the large ripples. Within experimental runs, ripple geometry did not vary greatly, the coefficient of variation (s.d./mean $\times 100\%$) ranged from 10% to 25% for λ and 30% to 40% for η . Although ripple geometry was similar between replicate experiments, it did change during the 15–16 h overnight deposition period. While there was no change in ripple wavelength (Table 1), the ripple crests became more rounded, and ripple height was reduced by 35–40% during this period most likely as a result of a bed compaction. Representative changes in ripple shape during the deposition period can be seen by comparing the bed profile in Fig. 4 (large ripples just formed) with that in Fig. 1c (large ripples after 15 h in depositional flows). Note, however, that these bed profiles are from separate experiments so the number of ripples, their size and location are not directly comparable between figures.

There were significant differences in the mean diatom deposition among bed types (flat, small and large ripples) and locations on rippled beds (crests and troughs; one-way ANOVA $p < 0.001$). Tukey's post-hoc tests indicated that mean diatom deposition was significantly less on the flat bed compared to the rippled beds but did not differ between small and large ripples (Table 2). For the small ripple treatment, the average bed chl *a* concentration from the two replicate experiments was $1.29 \mu\text{g chl } a \text{ cm}^{-2}$, the same as that recorded for the large rippled treatment and $\sim 1.6 \times$ greater than deposition to the flat bed (Table 2). Initial water-column chl *a* concentrations in the water tunnel did not vary appreciably among treatment runs (Table 1), and the mean deposition was remarkably consistent among replicate experiments (Table 2).

Extrapolating the mean bed chl *a* concentration measured in the centre of the working section (a strip 160 cm long \times 1 cm wide) to the entire bed (255 \times 21 cm) accounted for between 67% and 75% of the reduction in water-column chl *a* concentration. Although not systematically sampled, elevated chl *a* concentrations were observed in syringe cores collected at the edges adjacent to the walls of the sediment that could easily account for this shortfall. Note that these edge effects did not appear to have influenced results presented here, however, because diatom deposition was uniform to within 5 cm of the

tunnel walls (Fig. 1d and e, and discussed below) and our rates were derived from direct measurements of sediment chl *a* concentration as opposed to indirect estimates based on the reduction in water column chl *a* concentration which would have been influenced by deposition to other areas of the water tunnel.

Ripples not only increased total diatom deposition relative to the flat bed but also increased the spatial variability in deposited chl *a* (Table 2, Fig. 1). For the flat bed, diatoms were restricted to the sediment surface and were uniformly distributed along the length of the working section (Fig. 1a). For each rippled bed run, however, deposition was significantly higher (t -test $p < 0.01$ – 0.0001) in the troughs than on the crests (Table 2, Fig. 1b and c).

For the small rippled bed, mean chl *a* deposition in the troughs was $2.8 \times$ greater than on the crests whereas for the large ripple treatment this variation increased to $4.4 \times$ (Table 2). Mean chl *a* deposition in troughs was similar among rippled runs (one way ANOVA $p > 0.8$) but deposition to the crests did differ significantly ($p < 0.001$). Deposition to large crests was 45% lower than to small crests and post-hoc tests confirmed significant differences ($p < 0.05$) between small and large crest runs (but not between replicate runs as was anticipated; Table 2). The reduced deposition to the large crests accounts for the greater disparity between crests and troughs in the large rippled treatment compared to the small rippled treatment. Sampling between ripple crests and troughs produced intermediate values of chl *a* (Table 2). Cross-stream variations in diatom deposition were minimal (e.g. Fig. 1e and d) meaning that the along-stream sections (Fig. 1a–c) provided an accurate representation of the spatial distribution of bed chl *a* to within at least 5 cm of the water tunnel walls and that our data are free of any edge effects associated with the water tunnel walls.

In addition to the flux to the bed, ripples also affected the vertical penetration depth of diatoms into the sediment. In ripple troughs, chl *a* concentration per cm^3 of sediment decreased exponentially with depth but was still detectable at 4–5 cm below the sediment surface in both small and large ripple treatments (Fig. 2). On the crests, however, $> 94\%$ of the deposited chl *a* occurred in the upper cm of the sediment, and was not detectable at depths greater than 2 cm below the sediment surface. Similarly, for the flat bed treatment, the bulk of the chl *a* ($\sim 85\%$) occurred in the upper cm of the sediment and none below 2 cm (Fig. 2).

3.3. Effects of sediment transport on the bed diatom abundance and distribution

The abundance and distribution of diatoms deposited in the rippled beds proved to be highly

predictable (Tables 1 and 2, Figs. 1 and 2) allowing us to quantify any effects of the sediment transport in separate runs. The onset of large ripple formation after deposition to a small rippled bed quickly released diatoms into the water column (Fig. 3).

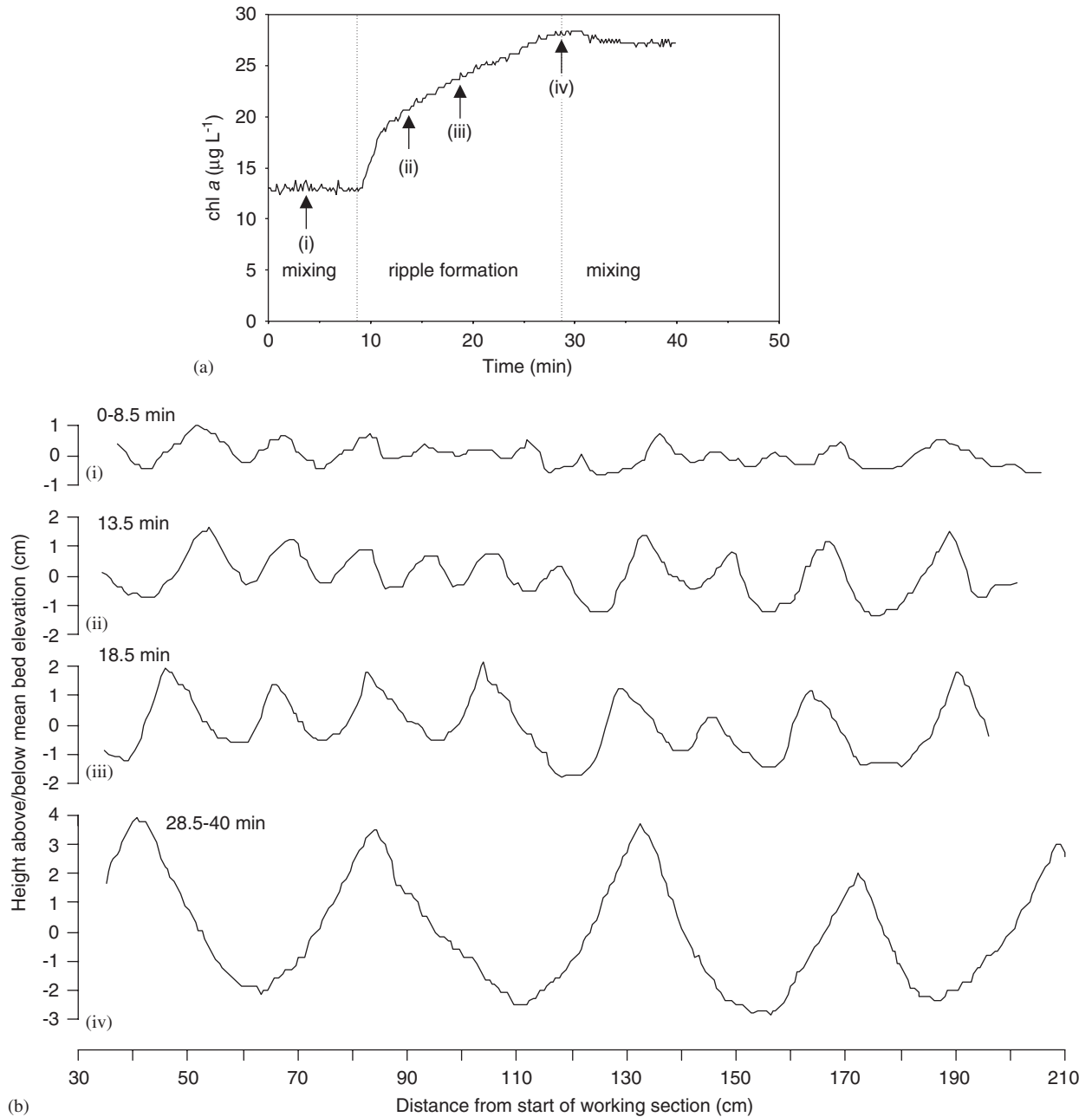


Fig. 3. (a) Concentration of diatoms ($\mu\text{g chl } a \text{ L}^{-1}$) in the water tunnel during a resuspension experiment as determined from *in vivo* fluorescence. The vertical dotted lines indicate the points where flow settings were altered from depositional to eroding (8.5 min) and back again (28.5 min). (b) Evolution of bed geometry during the resuspension experiment; (i) at the end of the deposition period (small ripple treatment), (ii) 5 min and (iii) 10 min after the start of sediment transport and (iv) the final bed configuration (large ripple treatment). To aid direct comparison, identical vertical scales are used in each plot.

In the first 5 min of sediment transport (interval indicated as (ii) in Fig. 3), mean ripple η had only increased from ~ 1 to 1.5 cm (λ remained constant) yet this was associated with a 55% of the total increase in water-column chl *a* concentration. By 10 min following the initiation of sediment transport ((iii) Fig. 3), ripple geometry changes to $\eta = 3$ cm and $\lambda = 18$ cm, and 75% of the total increase in water-column chl *a* concentration had occurred. Following the initial rapid release of bed diatoms, chl *a* concentration in the water column increased at a decelerating rate until the large ripples formed after 20 min ((iv) in Fig. 3). A reduction in the flow following the formation of the large ripples stabilized the chl *a* concentration in the water during (iv) in Fig. 3.

Not surprisingly, the resuspension and transport of sand resulting in the formation of large ripples reduced the concentration of diatoms in the sediment compared to the deposition experiments. The mean concentration of bed chl *a* at the end of the small ripple experiments ranged between 1.28 and 1.30 $\mu\text{g cm}^{-2}$ (Table 2) and at the end of the resuspension phase between 0.55 and 0.71 $\mu\text{g cm}^{-2}$ suggesting that 45–60% of the bed diatoms were transported into the water column during sediment transport. This assumes that the mean bed chl *a* concentration at the end of the depositional phase of the resuspension experiment was similar to that obtained for the small ripple experiments, a reasonable assumption given the similarity in experimental

conditions and reproducibility between replicate experiments (Tables 1 and 2).

Resuspension reduced the concentration of diatoms in the sediment and in addition markedly altered the distribution patterns established during depositional flows. The formation of large ripples resulted in peak chl *a* concentrations occurring beneath ripple crests rather than troughs and at depths of 2–4 cm below the sediment surface, rather than in the surface layer (0–1 cm) (Table 2, Fig. 4). Furthermore, beneath crests chl *a* was detected as deep as 6–7 cm (Fig. 5), effectively burying diatoms deeper into the sediment. Resuspension lowered chl *a* concentration in the troughs by 2.5–3.5 \times compared to the crests and was restricted primarily to the surface sediment (0–1 cm) layer (Table 2; Fig. 5). Sediment transport also increased the spatial variability in the distribution of bed diatoms. In depositional experiments to rippled beds, the distribution patterns of chl *a* were very consistent (Fig. 2) and also the variation in chl *a* concentration among troughs or crests within and between replicate experimental runs was relatively small (Table 2). In resuspension experiments this was not the case. For example, in Fig. 4, there was no chl *a* beneath one crest, yet beneath others, the amount, position relative to the crest and depth of burial, all varied. This is reflected in the increased variance about mean values compared to the depositional experiments (Table 2, compare Figs. 2 and 5).

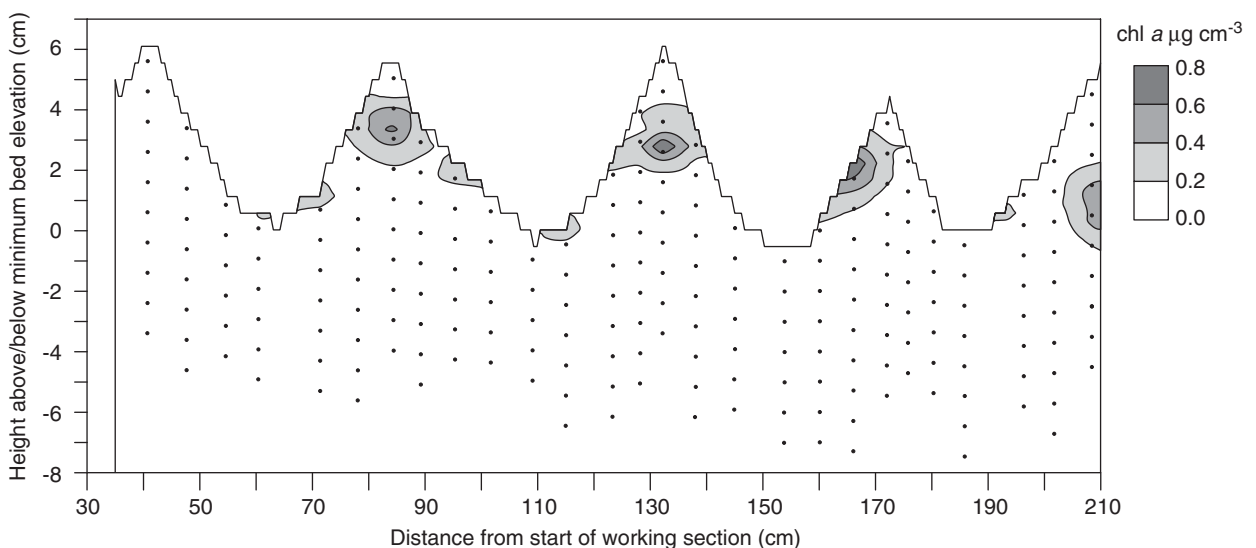


Fig. 4. Contour plot of the vertical distribution of sediment chl *a* at the end of a resuspension experiment. The plot was compiled from vertically sectioned sediment cores at the locations indicated by the black dots.

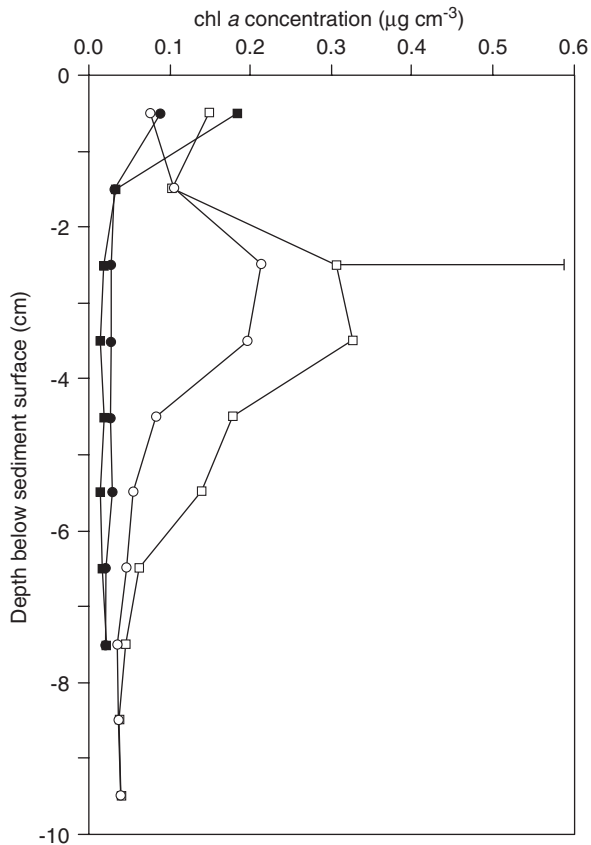


Fig. 5. Depth distribution of chl *a* in the troughs (solid symbols) and on the crests (open symbols) at the end of resuspension experiments. In each plot, the circle and square symbols refer to replicate experiments. Data represent the means of 5–9 sediment cores (see Table 2) and for clarity only the maximum s.d. has been shown, whereas the minimum s.d. is within the size of the symbol.

4. Discussion

4.1. Patterns of diatom deposition

The presence of ripples increased the spatial variability in deposited chl *a* compared to a flat bed (Table 2). Net deposition and the penetration of chl *a* into the bed was greater in the ripple troughs than on the ripple crests, a pattern that was highly repeatable between the replicated treatments and small and large ripples (Table 2). Although these diatom deposition patterns correlate with previous observations noting the visible accumulation of organic detritus in ripple troughs (e.g. Fenwick, 1984; Grant et al., 1986), the depositional processes differ. While the accumulation of comparatively large fragments of organic detritus is due to a reduction of bed shear stress in ripple troughs, in

our experiments, this reduction would not be sufficient to promote settling of near-neutrally buoyant diatom cells during our experimental runs.

The observed patterns of diatom deposition are consistent with the modelled (Shum and Sundby, 1996) and observed (Precht and Huettel, 2003, 2004; Precht et al., 2004; Reimers et al., 2004) porewater velocities generated when oscillating flow interacts with ripples. Higher flows over the ripple crests result in regions of lower pressure, and these horizontal pressure gradients produce fluid transport across the sediment–water interface that is directed into the bed in the troughs and flanks, and out of the bed on the crests (see Huettel and Webster (2001) for a review). Furthermore, our depositional patterns are also generally consistent with previous experiments conducted in unidirectional flows that have correlated spatial variations in POM deposition to permeable beds with the advective porewater exchange generated about biogenic roughness elements (Pilditch et al., 1998; Huettel and Rusch, 2000). The penetration depth of diatoms in ripple troughs (up to 4–5 cm) is comparable to those produced with unidirectional flows interacting with ripples or small mounds (Huettel and Rusch, 2000) and roughly twice as deep as those recorded to flat beds in situ (<3 cm; Rusch and Huettel, 2000) and in stirred cores (<2–3 cm; Ehrenhauss et al., 2004a, b).

4.2. Factors influencing diatom deposition rate

The deposition of diatoms will be governed both by the rate at which they are introduced to the upper layer of the sediment as well as the likelihood that they will be retained (Fries and Trowbridge, 2003). Within the bed (and between individual sand grains), fluid velocities drop dramatically with depth (Huettel et al., 1996), promoting gravitational deposition as well as increasing the probability of cells sticking to sand grains following inertial impaction or direct interception (Dade et al., 1991). In our case, however, gravitational deposition is unlikely to be a quantitatively important mechanism by which diatoms are delivered to the sediment surface. Diatom sinking velocities are in the order of 0.001 cm s^{-1} (e.g. Walsby and Reynolds, 1980), which is several orders of magnitude lower than velocities experienced in the water tunnel during the depositional flow treatment ($u_{bmax} = 13.7 \text{ cm s}^{-1}$). Turbulent conditions in the water tunnel will readily keep diatoms in suspension

and thus other processes are responsible for introducing diatoms in the surface layer of sediment.

In unidirectional flows, [Huettel and Rusch \(2000\)](#) observed a good agreement between the magnitude of diatom deposition about a single ripple and the rate of porewater exchange, suggesting that porewater exchange rate may be a good proxy for POM deposition. In oscillatory flows, ripples ($\eta = 0.7$ cm, $\lambda = 3$ cm) enhanced porewater exchange rates by factors of 6–15 times ([Precht and Huettel, 2003](#)), which is considerably higher than the differences we observed in the POM flux to flat and rippled beds ([Table 2](#)). This difference could be due to differences in experimental conditions. Although peak, near-bed, horizontal flow speeds were comparable between studies (11 vs. 14 cm s^{-1}), [Precht and Huettel's](#) waves were of a higher frequency and the ripple steepness (η/λ) was greater, all factors which promote greater porewater advective exchange ([Shum, 1992; Huettel and Webster, 2001](#)). In our experiments, we measured deposition to a fully rippled bed and although diatom deposition was enhanced in the troughs compared to the flat bed there was also reduction on the crests (cf. [Huettel and Rusch, 2000](#)). Nevertheless, the fact that we did not see a difference in the diatom flux between the small and large ripple treatments, and a comparatively small difference between rippled and flat bed treatments does suggest that advective porewater exchange driven by pressure gradients may not be as important for net POM deposition as it is for solute exchange.

Two processes responsible for transferring diatoms into the bed that are likely to operate independently of bed roughness are interfacial water exchange caused by shear ([Beavers and Joseph, 1967](#)) and hydrostatic pressure oscillations or wave pumping ([Riedl et al., 1972; Harrison et al., 1983](#)). The high permeability of the sediment used in this study means that the boundary layer velocity profile will extend into the sand with shear generating porewater flows in the upper 2–3 mm of the sand ([Beavers and Joseph, 1967](#)). Flow dispersion within this layer will enhance fluid exchange with the overlying water ([Webster and Taylor, 1992](#)) and deliver POM to the bed even in the absence of ripples. These shear-generated porewater flows were probably responsible for the diatoms detected in the surface layer on ripple crests overcoming the pressure-induced porewater flows that exit the sediment at these locations. At the sediment surface,

the horizontal interstitial flows diverge under the wave crests and converge under the troughs. The diverging flow under the wave crest requires fluid to enter the sediment to maintain continuity and to leave the sediment under the wave troughs. A net solute transport is generated by shear ([Harrison et al., 1983](#)) and more importantly rotational dispersion ([Webster et al., 1996](#)) in the porewater that is many times more effective than molecular diffusion (reviewed by [Huettel and Webster, 2001](#)). In addition, the pressure oscillations in the wave tank along the working section ([Section 3.1](#)) will also drive porewater exchange. In this study, it appears that shear and potentially wave pumping may have accounted for a significant fraction of the POM flux to the bed so that the presence of ripples and the associated pressure gradients did not greatly increase total diatom deposition.

The less than expected differences in spatially integrated diatom deposition among treatments may also have been influenced by the duration of the experiment. The amount of phytoplankton retained by the bed will be dictated by the available void space (a function of grain size and packing) and once filled, further changes in bed diatom concentration will not occur. It is possible that at some point during the experiment, the high flux of diatoms to the troughs decreased sediment permeability to a point where further deposition could not occur. The time to reach this point may have differed between the ripple treatments, but the final bed diatom density will be determined by available void space, a factor that to first order (see porosity measurements above) was constant between treatments. If the rippled bed treatments had reached saturation during the experiments and the flat bed treatment (minus ripple generated pressure gradients) had not, then this may explain the limited difference in total deposition between rippled and flat beds (see [Table 2](#)). Without frequent measurements of water column chl *a*, we cannot discount this possibility, although [Pilditch et al. \(1998\)](#) using similar water-column concentrations of diatoms did not observe a change in deposition rates to coarse sands (mean grain size 615 and 1200 μm) during 22 h experiments.

Ripples not only create pressure gradients that influence porewater exchange but also increase the surface area over which diatoms can be deposited. It is difficult to determine the relative importance of these two processes as changes in ripple geometry simultaneously alter the surface area exposed to the

flow as well as pressure variations. However, our results cannot be explained solely in terms of surface area enhancement. Assuming that the ripples can be approximated by a sinusoid then compared to the flat bed treatment, the surface area of working section was enhanced by a factor of $1.75 \times$ and $2.15 \times$ for the small and large ripples, respectively. If surface area were the only factor regulating diatom deposition, then total deposition would increase with ripple size which was not observed and the mean deposition normalized by the surface area enhancement factor (which standardizes deposition to an equivalent area of sediment) would remain constant. In our experiments, this ratio decreased with increasing ripple size (flat bed = 0.8, small ripples = 0.74 and large ripples = 0.60) and is likely the result of advective porewater flows induced by the ripples. It is important to note that although ripples increase the surface area exposed to flow, they also generate regions of high and low diatom accumulation in the sediment, and this result cannot be explained simply by increased bed area alone.

4.3. Resuspension modifies vertical pattern of POM incorporation into sediments

As expected, we found high concentrations of diatoms with deeper penetration in ripple troughs (as compared to crests). Subsequent sediment transport reduced the bed diatom concentration by approximately 50% and the remaining diatoms were concentrated in sub-surface maxima several cm beneath ripple crests. This comparatively rapid and deep burial of diatoms is in contrast to low penetration depth of POM achieved during the 16 h depositional periods. This deeper burial may be significant in retaining POM in the sediments for longer periods since it is protected from transport events that disturb surface sediment layers and is likely to influence degradation rates (see below).

Previous studies have implicated sediment transport as an important process regulating phytoplankton POM concentrations in permeable sediments. *Jenness and Duineveld (1985)* observed resuspension and burial of chl *a* by tidal currents in North Sea sediments. During periods of slack water phytoplankton settled to the sediment surface and on the ebb tide flows were sufficient to cause ripple migration burying chl *a* to depths of 5 cm. On the other hand, peak flood flows were stronger and resuspended sediments eroded most of the chl *a*

from surficial sediments. While in this system the tidal cycle of deposition and resuspension was frequent, more commonly on continental shelves sediment transport is associated with waves generated by passing weather systems (e.g. *Traykovski et al., 1999*; *Lei and Amos, 1999*; *Hume et al., 2000*), and episodic burial events may be much more important in retaining POM. The subsurface maxima in phytoplankton distribution observed in this study have been observed in shelf (*Ehrenhauss et al., 2004a*) and intertidal sediments (*D'Andrea et al., 2002*) and were attributed to burial caused by sediment transport. *Grant et al. (1986)* also report that ripple migration buried surface diatom films by eroding intertidal sands in a unidirectional flume. Interestingly, the reduction of bed chl *a* following sediment transport (43–63%) was similar to that observed in this study. Our resuspension experiments suggest that on continental shelves POM distribution over days to weeks will reflect both deposition by advective porewater flows and burial caused by sediment transport.

While our measurements of diatom fluxes may have been affected by degradation during the deposition or physical abrasion during sediment transport, we believe these to be quantitatively unimportant. Regularly, we microscopically checked diatoms in suspension and in the sediment for ruptured cells and very few were observed. The sediment was devoid of fauna due to its source (dune sand) and our cleaning procedure between experiments, and algal cultures were supplied free of bacteria and viruses. Even if degradation were occurring, fresh diatom detritus in permeable continental shelf sands complete with fauna decays at a rate of 5–10% day⁻¹ (*Ehrenhauss et al., 2004a*). Although sediment transport was probably too short to directly influence diatom concentration (e.g. by abrasion of attached cells or disruption of live cells, *Miller, 1989*), it could be an important mechanism in situ accelerating POM degradation by fragmenting partially decayed particles and rupturing phytoplankton cells that lack silica frustules such as dinoflagellates.

The depositional flux of POM will vary with sediment permeability because of its controlling influence on the rate of porewater exchange with the overlying water column (*Huettler and Rusch, 2000*; *Fries and Trowbridge, 2003*). For example, *Pilditch et al. (1998)* observed a 7-fold increase in the diatom flux to a coarse (median grain dia. = 1200 μm) compared to a fine (170 μm) sand bed. Microbial

extracellular substances may also influence fine particle deposition via infilling voids (Meadows and Meadows, 1991) reducing sediment permeability or may even increase deposition if cells adhere to the organic films (Graham, 1990; Wang and Lee, 1993). However, biologically mediated effects may be reduced in regions that experience frequent resuspension events as grain abrasion can remove attached microbes (Miller, 1989). Although the magnitude of POM deposition will vary with sediment permeability, the depositional patterns associated with rippled, permeable beds are likely to remain.

4.4. Applicability of laboratory results to shelf conditions

We attempted to mimic sediment and hydrodynamic conditions representative of continental shelf environments. The grain size used in our experiments occurs on the continental shelf (e.g. Black and Oldman, 1999; Traykovski et al., 1999; Trembanis et al., 2004) and permeable sediments in general are widespread (Emery, 1968). Similarly, in water depths of 10 m, the water-tunnel eroding-flow conditions ($T = 8.8$ s, $u_{bmax} = 44$ cm s⁻¹) correspond to a wave height of 1.25 m whereas the depositional flows ($T = 13.5$ s, $u_{bmax} = 13.7$ cm s⁻¹) equate to a wave height of 0.3 m (estimated from linear wave theory, e.g. Dean and Dalrymple, 1992). In 30 m of water, the equivalent wave heights are 2.8 m and 0.7 m for the eroding and depositional flows, respectively. In comparison with the 9 years of wave data analysed by Traykovski et al. (1999) for the southern New Jersey continental shelf, the conditions we used in our experiments were certainly representative.

Likewise, ripple dimensions used in this study fall within those observed on continental shelves with comparable grain sizes. For example, during a 6-week instrument deployment at the LEO-15 site, ripple λ ranged from 10 to 100 cm with amplitudes up to 15 cm (Traykovski et al., 1999). Trembanis et al. (2004) recorded ripple heights of 2–25 cm and λ s of 20–100 cm for shallow sediments off Tairua, New Zealand. Ripples produced in wave tanks are often orbital (i.e. λ is proportional to near-bed orbital wave diameter) whereas in situ ripples tend to be anorbital with λ proportional to grain size (Wiberg and Harris, 1994). The large ripples produced in the wave tank have a steepness ($\eta/\lambda = 0.16$) characteristic of orbital ripples (0.17) whereas the steepness of

the small rippled treatments (~ 0.09) was considerably less and indicative of anorbital or suborbital ripples likely because the small ripples represented a transition to the large ripples in equilibrium with the water tunnel flow conditions. It is important to note that Traykovski et al. (1999) found ripple wavelength scaling with wave orbitals during storm events rather than median grain size, and they suggested that this discrepancy may be explained by some measure of the width of the grain size distribution. In any case, we will use the detailed field results of Traykovski et al. (1999) to further interpret our laboratory results.

4.5. POM patterns resulting from intermittent storm events

During calm conditions before a storm, POM will be deposited in the bed by the various mechanisms described above (Section 4.2). Deposition will be concentrated most deeply in ripple troughs (small and large ripple runs, Table 1 and Figs. 1 and 2, and Section 4.1, above), and significant amounts will accumulate in less than a day (cf. our 16-h experimental runs, Table 2). Since in the field, coarser sediments are found in ripple troughs (e.g. Hume et al., 2003), deposition there may be greater than our results suggest. Additionally, organic and inorganic materials will be deposited by gravitational settling because ripple troughs are areas of low shear stress, and over time leading to reduced permeability and diminishing advective input. In terms of total flux (see Section 4.2 above), permeable bed effects may be hard to distinguish from other mechanisms. Regardless, any pattern of localized POM will be determined largely by the surface ripples and other bedforms, while the amount deposited will be determined by the near-bed water-column concentration and time available for deposition with decreasing permeability and clogging eventually limiting amount of POM injected.

As storm-generated swells arrive from an approaching but still distant storm, near-bottom flows will increase in strength, orbital amplitude and period, and eventually the critical stress for sediment erosion will be reached. Resulting sediment transport will likely rearrange the bedforms into large and longer, orbital-scale ripples of wavelength correlated with near-bottom flows (see Traykovski et al., 1999, Fig. 10). Any POM in the active layer of sediment (that topmost layer in which individual

grains are alternatively buried, re-exposed and transported as ripples migrate or change profile) will be released rapidly, suspended high above the bed and presumably washed downstream (resuspension experiment, Fig. 3a, time points (ii) through (iv)). From the movement of sand particles, new ripple crests will form (resuspension, Fig. 3b) or existing ones may migrate in the direction of the net flow, and this will bury deeper any POM in the sediment below the active depth. At the peak of the storm, intense sediment movement creates active ripples low in POM over the buried pattern of POM from previous ripples. As long as the active depth does not exceed the depth of burial, a relict or fossil pattern of elevated POM concentration will remain in the sediments.

As the storm subsides, surface wave height and period both decrease, and ripple wavelength remains the same (or may decrease, e.g. Traykovski et al., 1999, Fig. 10), and sediment movement will subside. We expect any rearrangement of the surface active layer will occur without deepening of the depth of erosion. POM patterns formed before the storm are thus preserved under a newly rippled surface bearing little or no resemblance to the pre-storm bed (resuspension experiment, Figs. 4 and 5). During relatively calm conditions (i.e. without sediment movement), POM will again be deposited to the bed as described above, but focused along the troughs of the newly formed ripples. The resulting superimposed, crisscrossing pattern (relative orientation depending on the mean currents during successive storm events) will be a superposition of elevated POM with older POM decreasing due to microbial remineralization, deposit feeding and bioturbation (processes not investigated here, and well beyond the scope of our experiments). This scenario, employing straight, two-dimensional ripples, is simplest consistent with our laboratory and recent field results (as cited here), while transitions to more three-dimensional patterns (sinuous, linguoid, cusped or branching) would impose further heterogeneity. Clearly, alternating calm (depositional) and storms (erosive, potential POM loss) periods will cause substantial horizontal heterogeneity in POM and localized concentrations with depth—both of which may be weakly or wholly unrelated to the existing surface topography. Any correlation between sediment POM and bedforms depends critically on the time of sampling relative to prior sediment transport events.

The above scenario follows that of storm events at a shallow continental shelf site similar to that modelled in our experiments. However, note that our resuspension runs represented a restricted set of possible conditions, and that removal consequently could well be greater than we estimated: as ripples migrate, essentially all POM initially buried beneath the crests could be exposed and lost from the bed (Jenness and Duineveld, 1985; Grant et al., 1986). Under intense storm conditions, ripples can be washed out completely and upper-plane bed sheet flow occurs (Li and Amos, 1999), which would remove much of the low-density POM from the surface sediments. Nevertheless, as the storms abate and ripples form, they will influence a subsequent, new flux of POM to the bed. Overall this conclusion, that intermittent events lead to substantial and spatially complex POM heterogeneity, is robust and not dependent on any particular bedform shape, size (in relation to flow, i.e. orbital vs. anorbital ripples) or influence of tidal flows in combination with waves. Rapid ripple movement and reconfiguration interspersed with longer, inter storm depositional intervals will drive POM inputs and patterns in shelf sediments.

4.6. *Geochemical and ecological implications*

The spatial distribution of POM in permeable beds observed in this study is likely to play an important role in remineralization. Advected pore-water velocities control the distribution of oxygen in rippled beds with oxic porewaters penetrating deeper beneath troughs and anoxic porewater drawn from deeper in the sediments exiting from ripple crests (Precht et al., 2004). During periods of calm weather POM deposition to ripple troughs will coincide with high oxygen concentrations promoting aerobic mineralisation whereas POM buried beneath crests (Figs. 4 and 5) is more likely to undergo anaerobic decomposition. The pathway of decomposition strongly influences mineralization rates and release of dissolved inorganic nutrients (Aller, 1994; Gunnars and Blomqvist, 1997; Kristensen and Holmer, 2001). It is recognized that permeable sediments can be sites of rapid organic matter degradation (e.g. Rowe et al., 1988; Grant et al., 1991; Reimers et al., 2004), and this has been widely suggested as a reason for their generally low organic content (e.g. Shum and Sundby, 1996). In core incubation experiments, Ehrenhauss et al. (2004b) observed that 5–10% of the nitrogen added

to permeable sediments in the form of diatoms was regenerated during the first day. In situ the simultaneous supply of labile POM and oxygen to ripple troughs may further enhance these decomposition rates. During sediment transport oxygen distribution is controlled by the rate of ripple migration. At low rates of ripple migration ($<10\text{ cm h}^{-1}$), porewater distribution migrates with the ripple crests whereas under high rates of ripple migration, the entire sediment surface layer is oxic (Precht et al., 2004). Oxygen distribution in the sediments is itself likely to be modified further by the reduction in POM resulting from sediment transport.

Our tracer was a small diatom representative of shelf primary producers, and this labile form of POM is likely to be a significant energy source for benthic ecosystems (Wollast, 1991; Buscail et al., 1995; Olesen and Lundsgaard, 1995). Regions of high POM concentration that accumulate in ripple troughs during periods of low flow and under ripples crests following sediment transport may serve as an important food source for benthic fauna. Several studies have examined the relationship between faunal distribution and ripples for intertidal, shallow sub-tidal and shelf sites. Hogue and Miller (1981) demonstrated that peaks in nematode density were associated with sediment crests at depths equal to the troughs. Those authors suggest that this pattern resulted from nematodes initially attracted to organic matter accumulating in the troughs but had subsequently been buried by migrating ripples. Similarly, Grant (1981) also observed a relationship between bedforms and fauna on an intertidal sand flat with crustaceans more abundant under crests than troughs. In a detailed study of habitat partitioning, Fenwick (1984) reported that predatory amphipods were concentrated beneath ripple crests associated with meiofauna prey, whereas sand-browsing amphipods were more concentrated in ripple troughs, both predictable responses to food supply. Subtidally, Barros et al. (2004) noted that macrofauna density was greater in troughs than on ripple crests at three of the four sites sampled. These authors stressed they could not determine whether these patterns were caused by passive accumulation in regions of low stress or represented active migration in response to other cues. Finally, Sedlacek and Thistle (2006) observed greater percent emergence from ripple crests in 3 of 12 species of harpacticoid copepods at a 20-m deep site off the Florida

panhandle. It is clear from these studies that microhabitat differences between ripple crests and troughs are significant to many benthic fauna, and we suggest that these responses may be in part related to the pattern of POM deposition investigated herein.

5. Conclusion

Our results indicate that deposition on a rippled bed exhibits a simple pattern predicted by models and past experimental work. However, the total particulate flux may be, in comparison, less directly controlled by advective porewater flow driven by bedforms since other mechanisms are capable of incorporating particles in the bed. Furthermore, we demonstrate that the long-term spatial patterns of deposition in permeable shelf sediments will be largely determined by both local sediment erosion and deposition. Thus, these two processes act in tandem to lead to substantial, ripple scale heterogeneity (both vertically and horizontally) of organic matter input to shelf sediments. Such spatial and temporal variations will likely influence remineralization within the sediments as well as the benthic infauna that inhabit them.

Acknowledgements

We thank A. Bradley for assistance with the experiments. C. Sommerfield and D. Hutchins kindly loaned us analytical equipment and K. Bryan provided the rectification software. The constructive criticism of two anonymous reviewers and discussions with A. Trembanis regarding storm events and sediment transport in shallow-water environments improved the manuscript. R. Dale and J. Brown provided additional comments. This project was funded by the University of Delaware College Sea Grant Program Project R/ME-31 to W.J. Ullman and D.C. Miller, which is gratefully acknowledged.

References

- Aller, R., 1994. Bioturbation and remineralization of sedimentary organic matter: effects of redox oscillation. *Chemical Geology* 114, 331–345.
- Andrews, D., Bennett, A., 1981. Measurements of diffusivity near the sediment–water interface with a fine-scale resistivity probe. *Geochimica Cosmochimica Acta* 45, 2169–2175.
- Barros, F., Underwood, A.J., Archambault, P., 2004. The influence of troughs and crests of ripple marks on the

- structure of subtidal benthic assemblages around rocky reefs. *Estuarine, Coastal and Shelf Science* 60, 781–790.
- Beavers, G.J., Joseph, D.D., 1967. Boundary conditions at a neutrally permeable wall. *Journal of Fluid Mechanics* 30, 197–207.
- Berner, R.A., 1980. *Early Diagenesis: A Theoretical Approach*. Princeton University Press, Princeton, NJ.
- Black, K.P., Oldman, J., 1999. Wave mechanisms responsible for grain sorting and on-uniform ripple distribution across two moderate-energy, sandy continental shelves. *Marine Geology* 162, 121–132.
- Buscail, R., Pocklington, R., Germain, C., 1995. Seasonal variability of the organic matter in a sedimentary coastal environment: sources, degradation and accumulation (continental shelf of the Gulf of Loins, northwest Mediterranean Sea). *Continental Shelf Research* 15, 843–869.
- Canfield, D.E., Thamdrup, B., Hansen, J.W., 1993. Pathways of organic carbon oxidation in three continental margin sediments. *Marine Geology* 113, 27–40.
- D'Andrea, A.F., Aller, R.C., Lopez, G.R., 2002. Organic matter flux and reactivity on a South Carolina sandflat: the impacts of porewater advection and macrobiological structures. *Limnology and Oceanography* 47, 1056–1070.
- Dade, W.B., Nowell, A.R.M., Jumars, P.A., 1991. Mass arrival mechanisms and clay deposition at the seafloor. In: Bennett, R.H., Bryant, W.R., Hulbert, M.H. (Eds.), *Microstructure of Fine-grained Sediments*. Springer, New York, pp. 161–165.
- Dean, R.G., Dalrymple, R.A., 1992. *Water Wave Mechanics for Engineers and Scientists*. Prentice-Hall, Englewood Cliffs, New Jersey, 353p.
- Eckman, J.E., 1990. A model of passive settlement by planktonic larvae onto bottoms of different roughness. *Limnology and Oceanography* 35, 887–901.
- Ehrenhauss, S., Witte, U., Bühring, S.I., Huettel, M., 2004a. Effect of advective porewater transport on distribution and degradation of diatoms in permeable North Sea sediments. *Marine Ecology Progress Series* 271, 99–111.
- Ehrenhauss, S., Witte, U., Janssen, F., Huettel, M., 2004b. Decomposition of diatoms and nutrient dynamics in permeable North Sea sediments. *Continental Shelf Research* 24, 721–737.
- Emery, K.O., 1968. Relict sediments on continental shelves of the world. *American Association of Petroleum Geologists Bulletin* 52, 445–464.
- Fenchel, T., 1996. Worm burrows and oxic microniches in marine sediments. 1. Spatial and temporal scales. *Marine Biology* 127, 289–295.
- Fenwick, G.D., 1984. Partitioning of a rippled sand habitat by five infaunal crustaceans. *Journal of Experimental Marine Biology and Ecology* 83, 53–72.
- Forster, S., Huettel, M., Ziebis, W., 1996. Impact of boundary layer flow velocity on oxygen utilization in coastal sediments. *Marine Ecology Progress Series* 143, 173–185.
- Fries, J.S., Trowbridge, J.H., 2003. Flume observations of enhanced particle deposition to permeable beds. *Limnology and Oceanography* 48, 802–812.
- Graf, G., Rosenberg, R., 1997. Bioresuspension and biodeposition: a review. *Journal of Marine Systems* 11, 269–278.
- Graham, A.A., 1990. Siltation of stone-surface periphyton in rivers by clay-sized particles from concentrations in suspension. *Hydrobiologia* 199, 107–115.
- Grant, J., 1981. sediment transport and disturbance on an intertidal sandflat: infaunal distribution and recolonisation. *Marine Ecology Progress Series* 6, 249–255.
- Grant, J., Bathmann, U.V., Mills, E.L., 1986. The interaction between benthic diatom films and sediment transport. *Estuarine, Coastal and Shelf Science* 23, 225–238.
- Grant, J., Emerson, C.W., Hargrave, B.T., Shortle, J.L., 1991. Benthic oxygen consumption on continental shelves off eastern Canada. *Continental Shelf Research* 11, 1083–1097.
- Grant, J., Cranford, P., Emerson, C., 1997. Sediment resuspension rates, organic matter quality and food utilization by sea scallops (*Placopecten magellanicus*) on Georges Bank. *Journal of Marine Research* 55, 965–994.
- Guillard, R.R.L., Kilham, P., 1977. The ecology of marine planktonic diatoms. *Botanical Monographs* 13, 372–469.
- Gunnars, A., Blomqvist, S., 1997. Phosphate exchange across the sediment–water interface when shifting from oxic to anoxic conditions—an experimental comparison of freshwater and brackish-marine sediments. *Biogeochemistry* 37, 203–226.
- Hargrave, B.T., 1973. Coupling carbon flow through some pelagic and benthic communities. *Journal of the Fisheries Research Board of Canada* 30, 1317–1326.
- Harris, P.T., Coleman, R., 1998. Estimating global shelf sediment mobility due to swell waves. *Marine Geology* 150, 171–177.
- Harrison, W.D., Musgrave, D., Reeburgh, W.S., 1983. A wave-induced transport process in marine sediments. *Journal of Geophysical Research* 88, 7617–7622.
- Heikkila, J., Silven, O., 1996. Calibration procedure for short focal length off-the-shelf CCD cameras. In: *Proceedings of the 13th International Conference on Pattern Recognition*. Vienna, Austria, pp. 166–170.
- Hogue, E.W., Miller, C.B., 1981. Effects of sediment microtopography on small-scale spatial distributions of meiobenthic nematodes. *Journal of Experimental Marine Biology and Ecology* 53, 181–191.
- Horne, E.P.W., Loder, J.W., Harrison, W.G., Mohn, R., Lewis, M.R., Irwin, B., Platt, T., 1989. Nitrate supply and demand at the Georges Bank tidal front. *Topics in Marine Biology* 53, 145–158.
- Huettel, M., Rusch, A., 2000. Transport and degradation of phytoplankton in permeable sediment. *Limnology and Oceanography* 45, 534–549.
- Huettel, M., Webster, I.T., 2001. Porewater flow in permeable sediments. In: Boudreau, B.P., Jørgensen, B.B. (Eds.), *The Benthic Boundary Layer: Transport Processes and Biochemistry*. Oxford University Press, Oxford, pp. 144–179.
- Huettel, M., Ziebis, W., Forster, S., 1996. Flow induced uptake of particulate matter in permeable sediments. *Limnology and Oceanography* 41, 309–322.
- Hume, T.M., Oldman, J.W., Black, K.P., 2000. Sediment facies and pathways of sand transport about a large deep water headland, Cape Rodney, New Zealand. *New Zealand Journal of Marine and Freshwater Research* 34, 695–717.
- Hume, T.M., Trembanis, A.C., Hill, A., Lifting, R., Stephens, S., 2003. Spatially variable, temporally stable, sediment facies on an energetics inner shelf. In: *Coastal Sediments '03*. ASCE Press, Clearwater Beach, FL, 14pp.
- Jackson, P.D., Taylor-Smith, D., Stanford, P.N., 1978. Resistivity–porosity–particle shape relationships for marine sediments. *Geophysics* 43, 1250–1268.

- Jenness, M.I., Duineveld, G.C.A., 1985. Effects of tidal currents on chlorophyll a content of sandy sediments in the southern North Sea. *Marine Ecology Progress Series* 21, 283–287.
- Jørgensen, B.B., 1977. Bacterial sulfate reduction within reduced microniches of oxidized marine sediments. *Marine Biology* 41, 7–17.
- Jørgensen, B.B., Bang, M., Blackburn, T.H., 1990. Anaerobic mineralization in marine sediments from the Baltic Sea–North Sea transition. *Marine Ecology Progress Series* 59, 39–54.
- Klute, A., Dirksen, C., 1986. Hydraulic conductivity and diffusivity: laboratory methods. In: Klute, A. (Ed.), *Methods of Soil Analysis, Part I. Physical and Mineralogical Methods*. American Society of Agronomy Monograph #9, second ed. pp. 687–700.
- Kristensen, E., Holmer, M., 2001. Decomposition of plant materials in marine sediments exposed to different electron acceptors (O_2 , NO_3^- and SO_4^{2-}), with emphasis on substrate origin, degradation kinetics, and the role of bioturbation. *Geochimica et Cosmochimica Acta* 65, 419–433.
- Li, M.Z., Amos, C.L., 1999. Field observations of bedforms and sediment transport thresholds of fine sand under combined waves and currents. *Marine Geology* 158, 147–160.
- Lofquist, K.E.B., 1977. A positive displacement water tunnel. Miscellaneous Report No. MR 77-1 to US Army, Corps of Engineers Coastal Engineering Research Centre, National Technical Information service, Springfield, Virginia.
- Meadows, P.S., Meadows, A., 1991. The geotechnical and geochemical implications of bioturbation in marine sedimentary ecosystem. *Symposia of the Zoological Society of London* 63, 157–181.
- Middelboe, M., Glud, R.N., Finster, K., 2003. Distribution of viruses and bacteria in relation to denitrification activity in an estuarine sediment. *Limnology and Oceanography* 48, 1447–1454.
- Miller, D.C., 1989. Abrasion effects on microbes in sandy sediment. *Marine Ecology Progress Series* 55, 73–82.
- Miller, D.C., Bock, M.J., Turner, E.J., 1992. Deposit and suspension feeding in oscillatory flows and sediment fluxes. *Journal of Marine Research* 50, 489–520.
- Miller, D.C., Norkko, A., Pilditch, C.A., 2002. Influence of diet on dispersal of horse mussel *Atrina zelandica* biodeposits. *Marine Ecology Progress Series* 242, 153–167.
- Nedwell, D.B., Parkes, R.J., Upton, A.C., Assinder, D.J., 1993. Seasonal fluxes across the sediment-water interface, and processes within sediments. *Philosophical Transactions of the Royal Society of London Series A. Physical Sciences and Engineering* 343, 519–529.
- Nowell, A.R.M., Jumars, P.A., 1984. Flow environments of the aquatic benthos. *Annual Review of Ecology and Systematics* 15, 303–328.
- Ölafsson, E., 1991. Small-scale distribution of marine meiobenthos: the effects of decaying macrofauna. *Oecologia* 90, 34–42.
- Olesen, M., Lundsgaard, C., 1995. Seasonal sedimentation of autochthonous material from the euphotic zone of a coastal system. *Estuarine, Coastal and Shelf Science* 41, 475–490.
- Parsons, T.R., Marit, Y., Lalli, C.M., 1984. *A Manual of Chemical and Biological Methods for Seawater Analysis*. Pergamon Press, Oxford, 173pp.
- Pilditch, C.A., Emerson, C.W., Grant, J., 1998. Effect of scallop shells and sediment grain size on phytoplankton flux to the bed. *Continental Shelf Research* 17, 1869–1885.
- Precht, E., Huettel, M., 2003. Advective pore-water exchange driven by surface gravity waves and its ecological implications. *Limnology and Oceanography* 48, 1674–1684.
- Precht, E., Huettel, M., 2004. Rapid wave-driven advective porewater exchange in a permeable coastal sediment. *Journal of Sea Research* 51, 93–107.
- Precht, E., Franke, U., Polerecky, L., Huettel, M., 2004. Oxygen dynamics in permeable sediments with wave-driven pore water exchange. *Limnology and Oceanography* 49, 693–705.
- Reimers, C.E., Stecher, H.A., Taghon, G.L., Fuller, C.M., Huettel, M., Rusch, A., Ryckelynck, N., Wild, C., 2004. In situ measurements of advective solute transport in permeable shelf sands. *Continental Shelf Research* 24, 183–201.
- Riedl, R., Huang, N., Machan, R., 1972. The subtidal pump: a mechanism of intertidal water exchange by wave action. *Marine Biology* 13, 210–221.
- Riggs, S.R., Snyder, S.W., Hine, C., Mearns, D.L., 1996. Hardbottom morphology and relationship to the geologic framework-Mid Atlantic continental shelf. *Journal of Sedimentary Research* 66, 830–846.
- Riley, G.A., 1956. *Oceanography of Long Island Sound, 1952–1954*. 9. Production and utilization of organic matter. *Bulletin of the Bingham Oceanography Collection* 15, 324–343.
- Rowe, G.T., Theroux, R., Phoel, W., Quinby, H., Wilke, R., Koschoreck, D., Whitledge, T.E., Falkowski, P.G., Fray, C., 1988. Benthic carbon budgets for the continental shelf south of New England. *Continental Shelf Research* 8, 511–527.
- Rusch, A., Huettel, M., 2000. Advective particle transport into permeable sediments: evidence from experiments in an intertidal sandflat. *Limnology and Oceanography* 45, 525–533.
- Sedlacek, L., Thistle, D., 2006. Emergence on the continental shelf: differences among species and between microhabitats. *Marine Ecology Progress Series* 311, 29–36.
- Shum, K.T., 1992. Wave-induced advective transport below a rippled water-sediment interface. *Journal of Geophysical Research* 97, 789–808.
- Shum, K.T., Sundby, B., 1996. Organic matter processing in continental shelf sediments—the subtidal pump revisited. *Marine Chemistry* 53, 81–87.
- Slama, C.C., Theurer, C., Henriksen, S.W., 1980. *Manual of Photogrammetry*. American Society of Photogrammetry, Falls Church, Virginia, 1056pp.
- Sleath, J.F.A., 1984. *Sea Bed Mechanics*. Wiley, New York, 335p.
- Smayda, T.H., 1970. The suspension and sinking of phytoplankton in the sea. *Oceanography and Marine Biology Annual Review* 8, 353–414.
- Snelgrove, P.V.R., Butman, C.A., 1994. Animal-sediment relationships revisited: cause versus effect. *Oceanography and Marine Biology Annual Review* 32, 111–177.
- Stolzenbach, K.D., Newman, K.A., Wong, C.S., 1992. Aggregation of fine particles at the sediment–water interface. *Journal of Geophysical Research* 97, 17889–17898.
- Thibodeaux, L.J., Boyle, J.D., 1987. Bedform-generated convective transport in bottom sediment. *Nature* 325, 341–343.
- Traykovski, P., Hay, A.E., Irish, J.D., Lynch, J.F., 1999. Geometry, migration and evolution of wave orbital ripples at LEO-15. *Journal of Geophysical Research* 104, 1505–1524.
- Trembanis, A.C., Wright, L.D., Friedrichs, C.T., Green, M.O., Hume, T., 2004. The effects of spatially complex inner shelf roughness on boundary layer turbulence and current and

- wave friction: Tairua embayment, New Zealand. *Continental Shelf Research* 24, 1549–1571.
- Turner, E.J., Miller, D.C., 1991. Behaviour and growth of *Mercenaria mercenaria* during simulated storm events. *Marine Biology* 111, 55–64.
- VanBlaricom, G.R., 1982. Experimental analysis of structural regulation in a marine sand community exposed to oceanic swell. *Ecological Monographs* 52, 283–305.
- Walsby, A.E., Reynolds, C.S., 1980. Sinking and floating. *The Physiological Ecology of Phytoplankton* 7, 371–412.
- Wang, X.C., Lee, C., 1993. Adsorption and desorption of aliphatic amines, amino acids and acetate by clay mineral and marine sediments. *Marine Chemistry* 44, 1–23.
- Webb, J.E., Theodor, J., 1968. Irrigation of submerged marine sands through wave action. *Nature* 220, 682–683.
- Webster, I.T., Taylor, J.H., 1992. Rotational dispersion in porous media due to fluctuating flow. *Water Resources Research* 28, 109–119.
- Webster, I.T., Norquay, S.J., Ross, F.C., Wooding, R.A., 1996. Solute exchange by convection within estuarine sediments. *Estuarine, Coastal and Shelf Science* 42, 171–183.
- Wiberg, P.L., Harris, C.K., 1994. Ripple geometry in wave dominated environments. *Journal of Geophysical Research* 99, 775–789.
- Wollast, R., 1991. The coastal organic carbon cycle: fluxes sources and sinks. In: Mantoura, R.F.C., Martin, J.-M., Wollast, R. (Eds.), *Ocean Margin Processes in Global change*. Wiley, New York, pp. 365–381.
- Yager, P.L., Nowell, A.R.M., Jumars, P.A., 1993. Enhanced deposition into pits a local food source for the benthos. *Journal of Marine Research* 51, 209–236.
- Zeldis, J., Oldman, J., Ballara, S., Richards, L., 2005. Physical fluxes, pelagic ecosystem structure and larval fish survival in the Hauraki Gulf, New Zealand. *Canadian Journal of Fisheries and Aquatic Sciences* 62, 561–593.